Multi-Shell Structured Fluorescent−Magnetic Nanoprobe for Target Cell Imaging and On-Chip Sorting
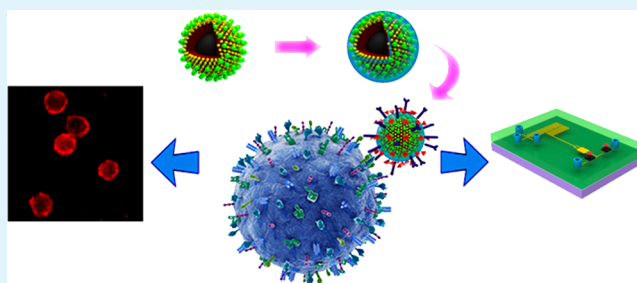
Peng-Hui Zhang, Jun-Tao Cao, Qian-Hao Min, and Jun-Jie Zhu*

State Key Laboratory of Analytical Chemistry for Life Science, School of Chemistry and Chemical Engineering, Nanjing University, Nanjing 210093, P.R.China

Ⓢ Supporting Information

ABSTRACT: In this paper, we have developed a core-triple-shell structured multi-functional nanoprobe $Fe_3O_4/SiO_2/CdSeTe@ZnS−SiO_2/polydopamine$ with strong fluorescence and a fast magnetic response for specifically recognizing, fluorescently labeling, and magnetically sorting target tumor cells on a microfluidic chip. The outer polydopamine layer not only effectively alleviated the quenching effect of the interlayer quantum dots but also provided a convenient and versatile functional interface to readily conjugate with the recognizing model molecules of aptamer KH1C12 with amine, thiol, or carboxyl groups. Moreover, the polydopamine isolation and PEG decoration equipped the as-fabricated nanoprobes with little cytotoxicity and nonspecific affinity, leading to the effective and specific profiling of the protein epitopes expressed on the target tumor cells. Taking advantage of the magnetic property and specific recognition, the modified nanoprobe was utilized to label and isolate HL-60 cells from a homogeneous cell mixture of HL-60 and K562 cells on a microfluidic chip. Combining with the high throughput of the microfluidic chip, 1.0×10^4 HL-60 cells were readily separated from 2.0×10^4 cells in only 10 min with 98% separation efficiency, markedly improved in comparison with conventional strategies. This study presents an innovative strategy for developing highly integrated nanoprobes of strong fluorescence and magnetic controllability, opening up a promising probe-based avenue for biological imaging and separation.

KEYWORDS: magnetic−fluorescent nanoprobe, polydopamine, cell imaging, cell sorting, microfluidic chip

■ INTRODUCTION

Cancer remains a great threat to human health because of its high morbidity and mortality.[1] Though current treatments based on surgery, radiation therapy, and chemotherapy have significantly improved the survival rate, the severe side effects bring worse suffering to the patients. In pursuit of higher efficacy, novel methods and techniques for accurate, sensitive, and rapid detection and targeted therapy of cancer have been developed. Recently, inorganic nanomaterials have been preferentially applied in tumor cell imaging, biosensing, targeted drug delivery, bioseparation, and biotherapy due to their variety of unique intrinsic properties, among which magnetism and fluorescence are the most attractive.[2−9] For the goal of labeling, tracking, and manipulating target tumor cells in vitro or in vivo, a new trend in developing multi-functional nanoparticles has emerged in the past few years.[10−14]

Up to now, plenty of magnetic and fluorescent nanoprobes have been designed and successfully applied in tumor cell targeting, sorting, drug delivery, and tumor therapy.[12,15,16] However, it is still an arduous task to fabricate the ideal nanoprobes possessing strong fluorescence, rapid magnetic response, and high specific recognition simultaneously. A crucial challenge is to avoid the fluorescent quenching effect while assuring magnetic performance of iron oxide and effective conjugation of biomolecules. To this end, many efforts have been devoted to alleviating the quenching by coating silica, polymer, or multi-layer polyelectrolyte on the magnetic core,[14,16−19] increasing the ratio of fluorophore to iron oxide,[20] or replacing the organic dye with quantum dots (QDs).[21] Meanwhile, massive strategies have been proposed for the functionalization of nanoprobes via electrostatic interactions with the help of polyelectrolyte or covalent linkage between amine and carboxyl using EDC/NHS.[20,22] However, the EDC/NHS system is too susceptible in aqueous solvent to get an ideal efficiency in surface bioconjugation, and an obvious quenching effect on quantum dots has also been observed.[23] Therefore, exploring an efficient route for building up multi-functional nanoprobes with both stable fluorescence and a modifiable surface is still in urgent demand for biological applications.
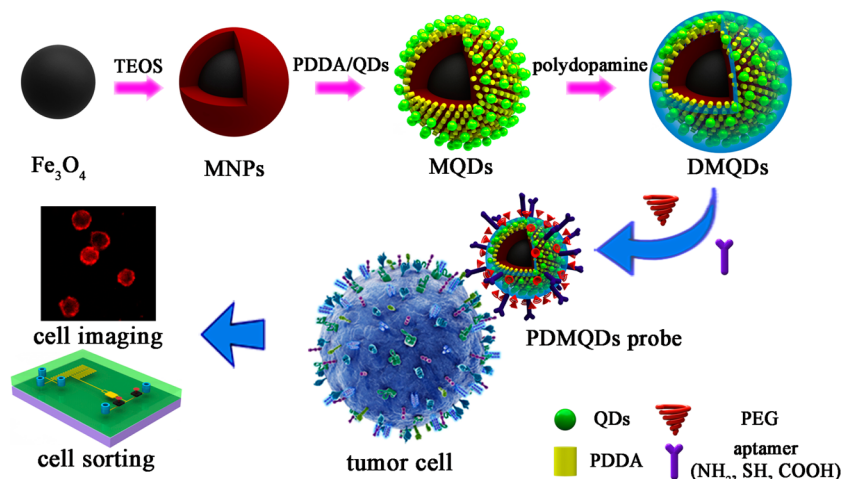
Nowadays, polydopamine is regarded as one of the most popular species in molecular modification not only for its convenience in combination with inorganic particles but also for its high reactivity with nucleophiles such as amine and thiol in alkaline medium.[24−27] However, as far as we know, such a feasible and versatile platform was rarely reported in

Scheme 1. Schematic Illustration of the Procedure for Fabrication and Application of Multi-Functional Nanoprobes

functionalizing quantum dots due to the misgivings about probable fluorescent quenching. Herein, we propose a novel type of mulit-shell structured multi-functional nanoprobe, composed of $Fe_3O_4/SiO_2/CdSeTe@ZnS-SiO_2/polydopamine$ core-triple-shell nanoarchitecture, which is favored for its high fluorescent intensity and rapid magnetic separation, as well as derivable polydopamine shell for biomolecular conjugation. As illustrated in Scheme 1, by means of the layer-by-layer assembly, the specific multi-functional nanoprobes were fabricated using an iron oxide core for magnetic manipulation, multi-layers of quantum dots for fluorescent imaging, polydopamine for biomolecular conjugation, aptamer for specific recognition, and PEG for long-term stability. Because of the strong fluorescence and high specificity, the aptamer-modified nanoprobes have sensitively evaluated the target protein expressed on the surface of tumor cells. Furthermore, the modified nanoprobes were applied in specifically labeling and sorting a leukemia cell line HL-60 from another cell line K562 in a microfluidic chip to get high separation efficiency in a short time.

EXPERIMENTAL SECTION

Materials and Reagents. Dopamine hydrochloride, tetraethyl orthosilicate (TEOS), 1-ethyl-3-(3-dimethylaminopropyl) carbodiimide hydrochloride (EDC), N-hydroxysuccinimide (NHS), and methoxypolyethylene glycol amine (PEG-NH$_2$, average MW 2 kD) were purchased from Sigma-Aldrich and used as received. Aptamer KH1C12 modified by amine, carboxyl, or thiol groups (denoted as aptamer-NH$_2$, aptamer-COOH, and aptamer-SH) were purchased from Shanghai Sangon Biological Engineering Technology & Services Co. (China). 3-(4,5-Dimethylthiazol-2-yl)-2,5-diphenyltetrazolium bromide (MTT) was obtained from Sunshine Biotech. Co. Ltd. (Nanjing, China). All other reagents were of analytical grade and used without purification. All aqueous solutions were prepared using ultrapure water from a Milli-Q system (Millipore, U.S.A.).

Synthesis of Fe$_3$O$_4$@SiO$_2$ Core–Shell Nanoparticles (MNPs). Typically, a cyclohexane solution of monodispersed Fe$_3$O$_4$ (30 μL) with a particle size of 22 nm prepared according to a reported work was dispersed in cyclohexane (46.2 mL) at room temperature under sonication.[28,29] Then, Triton X-100 (12.0 g), hexanol (9.6 mL), and H$_2$O (1.5 mL) were added with stirring to generate a microemulsion system. After 30 min, tetraethyl orthosilicate (TEOS, 50 μL) was added to the mixture. After reaction for 6 h, aqueous ammonia (28–30 wt %, 200 μL) was introduced to initiate the TEOS hydrolysis. After reaction for 16 h, acetone was added to destabilize the microemulsion system. The magnetic Fe$_3$O$_4$@SiO$_2$ composites were isolated via centrifugation and washed in sequence with ethanol and distilled water to remove surfactant and unreacted chemicals. The resultant core–shell composites were dispersed in distilled water (1 mL).

Preparation of Fe$_3$O$_4$@SiO$_2$@QDs (MQDs). CdSeTe@ZnS–SiO$_2$ quantum dots (QDs) were prepared according to our previous report.[30] As calculated from the HRTEM images in this work, the mean size of CdSeTe@ZnS–SiO$_2$ was about 5.0 nm, while the green-emitted CdSeTe core was about 3.9 nm with a lattice fringe of 0.36 nm, and the thickness of ZnS–SiO$_2$ shell was about 0.55 nm.[30] Then, Fe$_3$O$_4$@SiO$_2$@QDs was prepared by linking the negatively charged Fe$_3$O$_4$@SiO$_2$ and QDs with a positive polyelectrolyte through electrostatic interaction.[17] At first, Fe$_3$O$_4$@SiO$_2$ (1 mL) and PDDA solution (4 mL, 0.2 wt %, 0.5 M NaCl) were mixed under sonication for 30 min, and the excess polyelectrolyte was removed by centrifugation and washed with water. Afterward, the positively charged magnetic particles were dispersed into a QDs solution (3 mL, 0.1 M NaCl) and sonicated for 30 min. Then, MQDs coated with one layer of QDs were obtained by three centrifugation/washing cycles. MQDs coated with multi-layer QDs were prepared by repeating the above steps. The QDs amount coated on MQDs was estimated by determining the QDs concentration before and after assembly process. By monitoring the fluorescence variations of original QDs and supernatant, the QDs coated on per microgram MQDs was calculated as 10.2 nM mg^{-1}.

Preparation of Polydopamine-Coated MQDs (DMQDs). MQDs were dispersed in 10 mM pH 8.5 PBS (5 mL) containing dopamine (2.5 mg). The reaction solution was incubated by a shaking method for 30 min at 30 °C. Then, the reaction solution was subsequently centrifugated and washed with water to remove excess dopamine.

Functionalization of DMQDs and MQDs with Aptamer. Aptamer-NH$_2$, and aptamer-SH were applied in functionalizing DMQDs as follows. DMQDs were dispersed in pH 8.0 PBS containing aptamer-NH$_2$ (or aptamer-SH) and incubated by a shaking method at a speed of 200 rpm for 3 h. Then, the unreacted biomolecules were removed by three centrifugation/washing cycles. On the other hand, DMQDs were modified by aptamer-COOH through EDC/NHS coupling chemistry. At first, aptamer-COOH, EDC, and NHS were mixed in pH 7.0 PBS and incubated for 30 min to activate the terminal carboxyl group. Then, DMQDs were added into the solution, and the mixture was shaken for 3 h. The unreacted biomolecules were removed by three centrifugation/washing cycles.

MQDs-aptamer(NH$_2$) were modified by EDC/NHS coupling chemistry. MQDs, EDC, and NHS were mixed in pH 7.0 PBS and incubated for 30 min to activate the terminal carboxyl group. Then, aptamer-NH$_2$ was added into the solution, and the mixture was shaken for 3 h. The unreacted biomolecules were removed by three centrifugation/washing cycles.
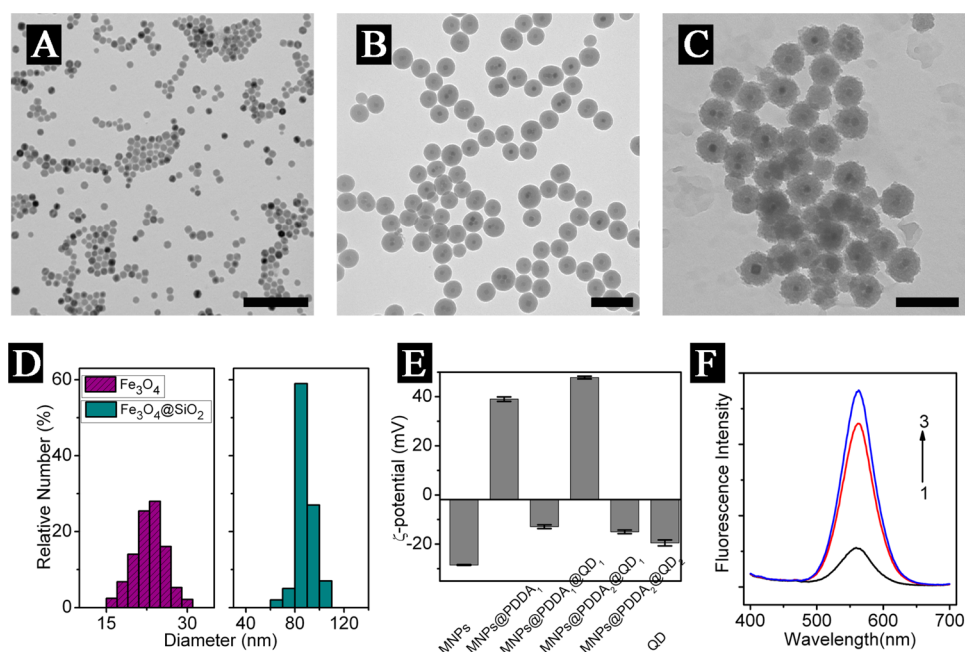
Figure 1. TEM images of (A) Fe_3O_4, (B) $Fe_3O_4@SiO_2$, and (C) MQDs. Scale bars, 200 nm. (D) Size distribution histograms of Fe_3O_4 and $Fe_3O_4@SiO_2$. (E) Zeta potential changes in the preparation of MQDs. (F) Fluorescence spectra of MQDs assembled with different layers of QDs.

Preparation of PEGylated DMQDs (PDMQDs). A purified concentrated solution of the functionalized DMQDs was treated with PEG-NH_2 stock solution (2 mg mL^{-1} in pH 8.0 PBS). The mixture was shaken for 3 h. The unreacted PEG-NH_2 molecules were cleaned by three centrifugation/washing cycles. Thus, PDMQDs-aptamer (NH_2, SH, and COOH) were obtained.

General Techniques. UV−vis spectra were recorded on a UV-3600 spectrophotometer (Shimadzu, Kyoto, Japan). Transmission electron micrographs (TEM) were measured on a JEOL JEM 200CX transmission electron microscope, using an accelerating voltage of 200 kV. A SQUID magnetometer (Quantum Design) was used for magnetic measurements at 300 K. Confocal laser scanning microscopy (CLSM) studies were performed using a Leica TCS SP5 microscope (Germany) with excitation at 405 nm. Fluorescence spectra were gained from a RF-5301PC spectrofluorophotometer (Shimadzu). Fluorescence images were acquired using a Nikon TE2000-U inverted fluorescent microscope equipped with a cooled CCD camera (DS-U1, Nikon Corporation, Japan). Dynamic light scattering (DLS) experiments were performed at 25 °C using a Brookhaven BI-200SM instrument, equipped with a He−Ne laser (632.8 nm) at a fixed scattering angle of 90°. Zeta potential was tested on a nano-z zeta potential analyzer (Malvern Instruments, U.S.A.). Flow cytometric analysis was recorded using FACS Calibur flow cytometer (Becton Dickinson, U.S.A.) and analyzed by WinMDI software (The Scripps Institute, La Jolla, CA).

Microfluidic Array Fabrication. The microfluidic device was fabricated using PDMS (Sylgard 184, Dow Corning) by the standard soft lithography method in accordance with our previous work.[31] Briefly, a photomask (printed at 10 000 dpi, Meijingwei Photoelectronics Co., Ltd., Suzhou, China) and negative photoresist SU-8 (Microchem, Newton, CA) based molds were used to fabricate the fluidic layer with the channel height of 50 μm. A thin layer of PDMS (10:1, elastomer to cross-linker ratio) was spin-coated onto the master and cured in 70 °C for 15 min. The prefabricated screw valve and silicone tubes (inlets and outlets) were manually pressed directly onto the SU-8 channel on the PDMS-coated master.[32] Then, PDMS was poured onto the mold to a thickness of 2 mm and cured in 70 °C for 2 h. At last, the fluidic layer was irreversibly bonded on a PDMS layer with a thickness of 500 μm to form a sealed device using an oxygen plasma treatment (Harrick Scientific Corporation, Ossining, NY). The microfluidic device was sterilized with 75% ethanol (v/v) and vacuumized for 3 min to eliminate air bubbles trapped in the channel. Following the ethanol treatment, 10 mM PBS (pH 7.4) was used to rinse the system for 3 min. Then, the device was incubated with 2% BSA in PBS at 37 °C for 30 min to block the channel surface to avoid nonspecific adsorption.

Cell Culture and Viability Assay. Human promyelocytic leukemia cells (HL-60 cells), human cervical carcinoma cells (Hela cells), and chronic myelogenous leukemia cells (K562 cells) were obtained from Nanjing KeyGen Biotech Co. Ltd. HL-60 cells and Hela cells were cultured in Dulbecco's Modified Eagle Medium (RPMI 1640 medium for K562 cells) at 37 °C under 5% CO_2 atmosphere, supplemented with L-glutamine (2 mM), penicillin (100 units mL^{-1}), streptomycin (100 μg mL^{-1}), and 10% fetal bovine serum (FBS). At the logarithmic growth phase, cells were collected and incubated with PDMQDs-aptamer (50 μg mL^{-1}) in a respective cultured medium without FBS. Cell viability was measured by MTT assay. Briefly, Hela cells were cultured on a 96-well plate at a density of 10000 cells each well. After 24 h incubation, the medium was replaced with 100 μL of fresh medium containing different concentrations of MQDs or PDMQDs (from 0 to 200 μg mL^{-1}). At the indicated time points (24 or 48 h), the medium was removed, and fresh medium (100 μL) containing MTT (20 μL, 5 mg mL^{-1}) was added into each well. After 4 h incubation, the optical density (OD) of the solution was measured to assess the relative viability of the cells using a Bio-Rad 680 microplate reader. Relative cell viability was expressed as ([OD]test/[OD]control) × 100%. Each experiment was repeated at least three times.

RESULTS AND DISCUSSION

Characterization of Magnetic and Fluorescent Nanocomposite. In order to obtain robust multi-functional nanoprobes, magnetic and fluorescent nanocomposites with uniform size and composition were prepared by layer-by-layer assembly. As shown in Figure 1A and Figure S1 of the Supporting Information, highly monodispersed Fe_3O_4 nanocrystals with average diameters of 22 nm were synthesized by the thermal decomposition of the metal-oleate precursors in a high boiling solvent. Then, $Fe_3O_4@SiO_2$ core−shell magnetic nanoparticles (MNPs) were obtained by employing Fe_3O_4 as a core and TEOS as a silica source via a reverse-microemulsion
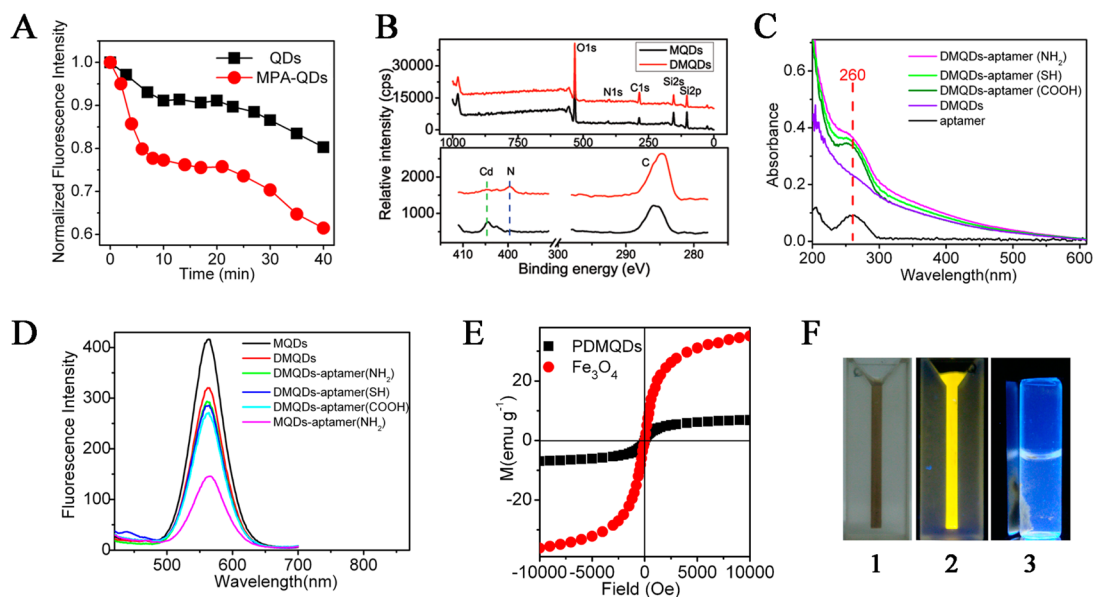
Figure 2. (A) Variation of fluorescence intensity in the assembly of dopamine onto MQDs coated with QDs (CdSeTe@ZnS−SiO$_2$) and MPA-QDs (CdSeTe@ZnS@CdS). (B) X-ray photoelectron spectrometry (XPS) spectra of MQDs and DMQDs. (C) UV−visible spectra of different nanoparticles and biomolecules (lines from top to bottom: DMQDs-aptamer(NH$_2$), DMQDs-aptamer(SH), DMQDs-aptamer(COOH), DMQDs, aptamer). (D) Fluorescence spectra of different nanoparticles (lines from top to bottom: MQDs, DMQDs, DMQDs-aptamer(NH$_2$), DMQDs-aptamer(SH), DMQDs-aptamer(COOH), MQDs-aptamer(NH$_2$)). (E) Field-dependent magnetization curves of Fe$_3$O$_4$ and PDMQDs at 300 K. (F) Photographs of PDMQDs in water before (1, 2) and after (3) attraction by a magnet for 10 min.

method. By controlling the concentration of Fe$_3$O$_4$ and the hydrolysis of TEOS, single core composites with tunable silica shells could be prepared. In this case, the iron oxide cores have a serious quenching effect on the QDs fluorescence through electronic coupling and energy transfer, and the broad absorbance spectrum of iron oxide also attenuates both the excitation light and emitted fluorescence.[33] Thus, thicker silica could enhance the fluorescent intensity by enlarging the distance between the QDs and iron oxide to prevent electron transfer, whereas the increase in silica would result in weakened magnetic response of the probe due to the diamagnetic contribution of the silica shell.[17,34−36] Finally, the diameter of MNPs and thickness of silica shell were, respectively, adjusted to 90 and 34 nm, and more than 80% composites entrapped single or double magnetic cores as shown in Figure 1B−D.

Afterward, CdSeTe@ZnS−SiO$_2$ QDs prepared in our previous work were deposited onto MNPs surface by layer-by-layer assembly to fabricate the magnetic quantum dots (MQDs) (Figure 1C).[30] The adoptive QDs exhibited an ultra high quantum yield with the aid of microwave heating in preparation process. Meanwhile, the ZnS−SiO$_2$ shell could efficiently prevent the Cd^{2+} release and enhance its photostability and water solubility. As illustrated in Figure 1E, the changes of zeta potentials during the preparation were used to monitor the assembly process. Driven by the electrostatic force, a uniform monolayer of positively charged PDDA and negatively charged QDs were alternately absorbed onto the negatively charged MNPs. As depicted in Figure 1F, MQDs continuously assembled with two layers of QDs exhibited a remarkable enhancement in fluorescent intensity compared to those with single layers, but the third QDs layer only led to a lesser increase. This phenomenon indicated that despite the isolated silica layer, the innermost layer of QDs still suffered from the quenching effect of the iron oxides. Thereby, the MQDs modified with two QDs layers were selected as the

optimal candidates for the construction of magnetic and fluorescent nanoprobes.

Bioconjugation of Magnetic and Fluorescent Nanoprobes. Having integrated magnetism and fluorescence in the nanocomposite, we next sought to fabricate the nanoprobes with recognizing molecules for target cell imaging and sorting. To conjugate the MQDs with different bioactive molecules, polydopamine was coated by mixing the MQDs and dopamine-hydrochloride in a basic buffer solution.[37] Notably, the thickness of polydopamine is a key issue for regulating the fluorescence, and thereby, the fluorescence variation was monitored during the polydopamine formation. As shown in Figure 2A, after the beginning drop caused by self-assembly of dopamine onto the QDs surface,[38,39] the fluorescent intensity of the MQDs reached a plateau, followed by a further decrease resulting from the oxidative polymerization of dopamine. Accordingly, the reaction time was set at 30 min to stave off further fluorescence quenching. The as-prepared DMQDs presented a quantum yield of 13 ± 2% by using rhodamine 6G as standard in Figure S2 of the Supporting Information. In comparison with the QDs (48 ± 2%) and MQDs (20 ± 1%), the decrease in DMQDs in quantum yield was attributed to the quenching effect and spectral absorption of iron oxide and the coating of the polydopamine. Even so, the fluorescence is high enough to fabricate nanoprobes for cell imaging. By replacing MQDs with mercaptopropionic acid (MPA)-capped QDs (CdSeTe@ZnS@CdS), which is negatively charged, a similar curve was observed. This phenomenon indicated that other negatively charged QDs also could be used to fabricate probes using the above assembly strategy. Compared with CdSeTe@ZnS@CdS, the stronger fluorescence intensity of PDMQDs prepared by CdSeTe@ZnS−SiO$_2$ suggests that the silica layer more efficiently passivates the quenching effect during the dopamine polymerization. Therefore, the thin polydopamine functional layer and highly fluorescent CdSeTe@ZnS−SiO$_2$ are

two vital factors in the fabrication of polydopamine-coated MQDs (DMQDs) with intense fluorescence. The X-ray photoelectron spectrometry spectra (XPS) in Figure 2B illustrated that after the dopamine polymerization, the nitrogen-to-carbon ratio of DMQDs was calculated as 0.118, which is similar to the theoretical value of dopamine (0.125), indicating the successful coating of polydopamine onto MQDs. Dynamic light scattering (DLS) experiments further confirmed the successful formation of the polydopamine shell. As shown in Figure S3 of the Supporting Information, the hydrodynamic diameters (HD) of $Fe_3O_4@SiO_2$, MQDs, and DMQDs were 96 ± 3, 127 ± 5, and 141 ± 5 nm, respectively, which were larger than the measured diameters from the TEM images. However, when the MQDs and dopamine reacted in distilled water, the MQDs−dopamine in Figure S4 of the Supporting Information exhibited a negligible variation in HD (130 ± 3 nm) because the dopamine molecules physically assembled onto MQDs without polymerization. It is hard to distinguish a 6 nm thick polymer shell in TEM (Figure S5, Supporting Information), where only smooth surfaces were observed.

In the case of bioconjugation, most of functional biomolecules, such as antibody, nucleic acid, peptide, and carbohydrate, possess amine, thiol, or carboxyl groups, which could be used to link with nanoparticles to fabricate probes. Thus, to investigate the convenience and versatility of polydopamine in nanoprobe functionalization, aptamer KH1C12 modified by different functional groups (aptamer-NH_2, aptamer-SH, and aptamer-COOH) were chosen as models to conjugate with DMQDs. In pH 8.0 PBS, the catechol of polydopamine was changed to o-quinone, showing a high reactivity with amine and thiol via the Michael addition or Schiff base reaction.[40] While in pH 7.0 PBS, aptamer-COOH could be linked with the physically assembled dopamine molecules using EDC/NHS method.[37] As shown in Figure 2C, the UV−visible spectra of DMQDs displayed a negligible characteristic absorbance peak of dopamine at 280 nm because only a thin layer of polydopamine was introduced in DMQDs. After the conjugation, the obvious absorbance around 260 nm could be observed, which was attributed to the characteristic absorbance band of the aptamer. Figure 2D presented the fluorescence spectra of the nanoparticles prepared by different methods. As a result of the dopamine polymerization, DMQDs exhibited a decrease in fluorescent intensity compared with MQDs but minor fluorescence decay occurred in the further modification of aptamer. By contrast, MQDs-aptamer(NH_2) linked by an EDC/NHS method saw a sharp fluorescence decline, proving that the polydopamine shell of DMQDs efficiently prevented QDs from being quenched by the reactants during the biomolecular modification. Furthermore, by covalently grafting amine-terminated methoxy-poly(ethylene glycol) (mPEG-NH_2) onto the polydopamine surface, the resulting PEGylated DMQDs (PDMQDs) displayed an increasing hydrodynamic diameter of 156 ± 8 nm (Figure S3, Supporting Information) and improved stability in PBS (Figure S6, Supporting Information). In addition, the field-dependent magnetism of PDMQDs (Figure 2E) was investigated by a superconducting quantum interference device (SQUID). No hysteresis was observed in the magnetization curve, exhibiting a superparamagnetic characteristic for PDMQDs. Their saturated magnetization decreased to 6.59 emu g^{-1} because the coating of the diamagnetic silica and QDs lowered the density of Fe_3O_4 in PDMQDs.[35] As shown in the separation test in Figure 2F, PDMQDs exhibited a rapid magnetic response that could be

attracted by a small magnet in 10 min. The above results suggest that the polydopamine shell provides a convenient coupling media for bioconjugation with aptamer and also an ideal protective shielding from quenching effect for the fluorescent nanoprobes.

In Vitro Cytotoxicity. To evaluate the cell toxicity of the nanoprobes, MTT tests were performed to reflect the integrity of the cell membrane and the damage extent on mitochondria function. As shown in Figure 3, Hela cells incubated with
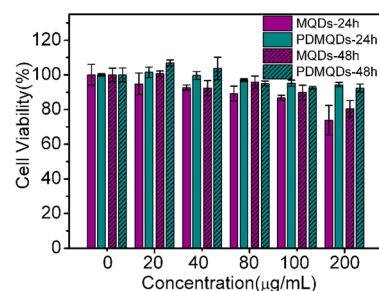

Figure 3. Viability of Hela cells incubated with MQDs or PDMQDs at different concentrations for 24 and 48 h. Data points are means ± standard deviations for three independent determinations.

MQDs and PDMQDs showed high viabilities, indicating their low toxicity to living cells. This phenomenon suggested that the ZnS−SiO$_2$ layers of CdSeTe@ZnS−SiO$_2$ quantum dots could efficiently prevent the leaking of Cd^{2+}, which is fatal to cell growth and proliferation.[30] In comparison with MQDs, PDMQDs showed almost no cytotoxicity to Hela cells because the strong chelating affinity of polydopamine to heavy metal ions could further avoid the release of Cd^{2+}. Particularly, the PEGylation might play an important role in reducing the nonspecific attachment of PDMQDs onto the cell surfaces and thus contribute to less endocytosis, a key factor for cytotoxicity.[41] The above deduction was confirmed by the confocal laser scanning microscopy (CLSM) images of Hela cells incubated with MQDs or PDMQDs for 24 h (Figure S7, Supporting Information). The intense fluorescent emitting showed that more MQDs were absorbed and taken up by the cells, while only a weak fluorescence was observed for PDMQDs. Meanwhile, the CLSM images also revealed that Hela cells maintained original morphology after treatment with PDMQDs for 24 h. The MTT and CLSM results indicated that PDMQDs possessed good biocompatibility, implying promising potential in biological application.

Specific Cellular Targeting with PDMQDs Nanoprobes. For either cell sorting or drug delivery, specific recognization to target cancer cells has been exploited for effective cancer therapies.[42] Aptamer KH1C12 is a desired candidate for fabricating specific nanoprobes because it possesses specific affinity to the target protein expressed on the surface of HL-60 cells but no recognition at all to most of T-cell and B-cell lines.[43] To assess the labeling efficiency and specificity of the fabricated nanoprobes in recognizing the target tumor cells, CLSM and flow cytometry were conducted. The prepared nanoprobes linked with aptamer-NH_2, aptamer-SH, and aptamer-COOH were incubated with HL-60 cells at 37 °C for 2 h. After removing the unbound nanoparticles by PBS washing, the confocal images were recorded as shown in Figure 4A. The cells incubated with MQDs-aptamer(NH_2) showed a weak fluorescence due to the poor fluorescent property of MQDs-aptamer(NH_2) resulting from the absence of polydop-
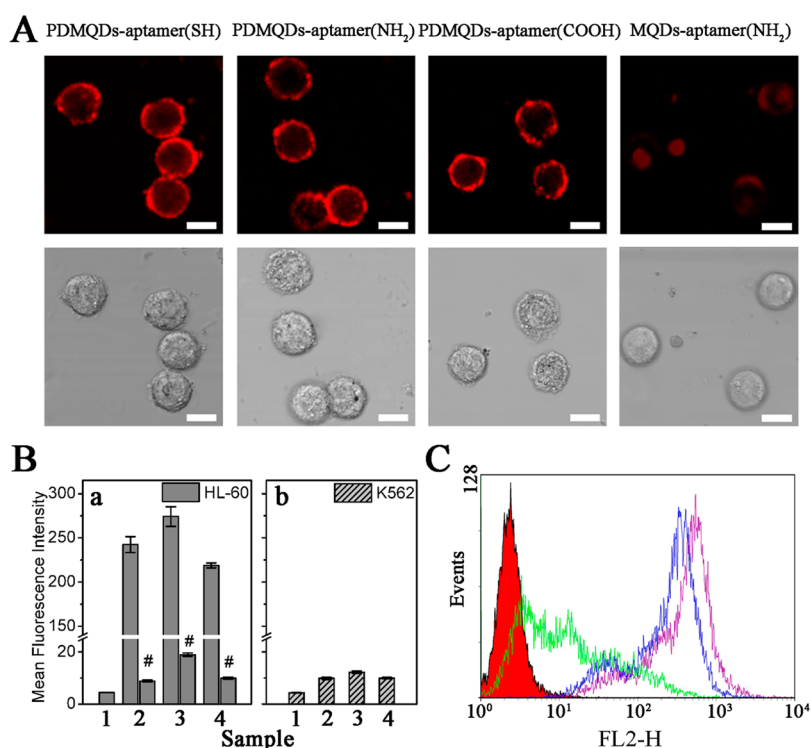
7421

dx.doi.org/10.1021/am401740a | *ACS Appl. Mater. Interfaces* 2013, 5, 7417−7424

Figure 4. Cellular targeting with PDMQDs-aptamer nanoprobes. (A) CLSM images of HL-60 cells incubated with PDMQDs-aptamer(SH), PDMQDs-aptamer(NH_2), PDMQDs-aptamer(COOH), and MQDs-aptamer(NH_2) after 2 h at 37 °C. Scale bars, 10 μm. (B) Variation of mean fluorescence intensities obtained from flow cytometry for (a) HL-60 and (b) K562 cells incubated with (2) PDMQDs-aptamer(SH), (3) PDMQDs-aptamer(NH_2), and (4) PDMQDs-aptamer(COOH). Cells incubated in culture medium without any probes were employed as (1) control. The data bars labeled by # in (a) mean competitive assays in which cells were treated with 10-fold excess of KH1C12 aptamer before incubating with nanoprobes. Data points are means ± standard deviations for three independent determinations. (C) Flow cytometry analysis of HL-60 cells incubated with different bioconjugates (from left to right: control, PDMQDs, DMQDs, and PDMQDs-aptamer(NH_2)).

amine isolation layer. In comparison, all the PDMQDs nanoprobes have effectively labeled the target protein expressed on the surface of HL-60 cells to yield a bright, uniform, ring distribution of fluorescence. To clarify the role of the aptamer in cell labeling, competitive assays were performed by treating HL-60 cells with 10-fold excess of aptamer molecules to saturate the recognizing protein on cell surfaces. As shown in Figure 4B, the fluorescent intensity of flow cytometry in the competitive assay shows an obvious decrease, suggesting the vital role of the aptamer in the recognition. Meanwhile, K562 cells were employed as a control to investigate the specificity of the PDMQDs-aptamer probes.[43] The weak fluorescence emitted from K562 cells reflected the high exclusivity of the nanoprobes to HL-60 cells. From the excellent specific recognition of the PDMQDs nanoprobes, it was concluded that the aptamer molecules were efficiently conjugated onto the nanoprobes, and their recognizing capability were retained. The nonspecific adsorption of the prepared nanoprobes was also evaluated by flow cytometry. As shown in Figure 4C, the cells of DMQDs group display a high fluorescent intensity, while a weak fluorescent emitting is observed in PDMQDs group, which suggested that the introduction of PEG brought an obvious decrease in nonspecific interaction between nanoprobes and cells. Furthermore, in the photostability test (Figure S8, Supporting Information), the nanoprobes labeled on the cell surfaces displayed excellent photochemical stability in 24 h as a consequence of the polydopamine protective layer.[21] After modification with polydopamine, PEG, and target biomolecules, the multi-functional nanoprobes were built up to be a

combination of strong fluorescence, excellent photostability, and high resistance to nonspecific adhesion for target tumor cell recognition.

On-Chip Isolation of Target Tumor Cells with PDMQDs Nanoprobes. To date, fluorescence-activated cell sorting (FACS) and magnetic-activated cell sorting (MACS) have been developed in cell analysis with the aids of immuno-fluorescent probes or immuno-magnetic probes.[44−47] Nevertheless, both of FACS and MACS are expensive, voluminous, complicated, and time-consuming, far from rapid and efficient analysis of minute sample.[47] Fortunately, the emergence of microfluidic devices brought out good news for cell sorting due to their inherent advantages with respect to minute sample consumption, reduced analysis time, and lower cost.[48−53] By the integration of corresponding functional units, labeling, sorting, and counting the target cells could be co-realized in a single chip on the basis of multi-functional nanoprobes.

In our case, a smart microfluidic system was devised to highlight the remarkable performance of PDMQDs nanoprobes in cell imaging and sorting. As illustrated in Figure 5A and B, PDMQDs-aptamer, HL-60, and K562 cells were simultaneously loaded into the three inlets by a peristaltic pump. A periodic serpentine channel was designed to accelerate the mixing velocity and increase the incubation time between cells and probes.[54] At an appropriate flow rate, the HL-60 cells labeled by the nanoprobes were trapped in the sorting chamber under the magnetic force, while K562 cells were flowed to the right outlet. After the external magnet was removed, the HL-60 cells could be carried to the left outlet by switching the screw valves.
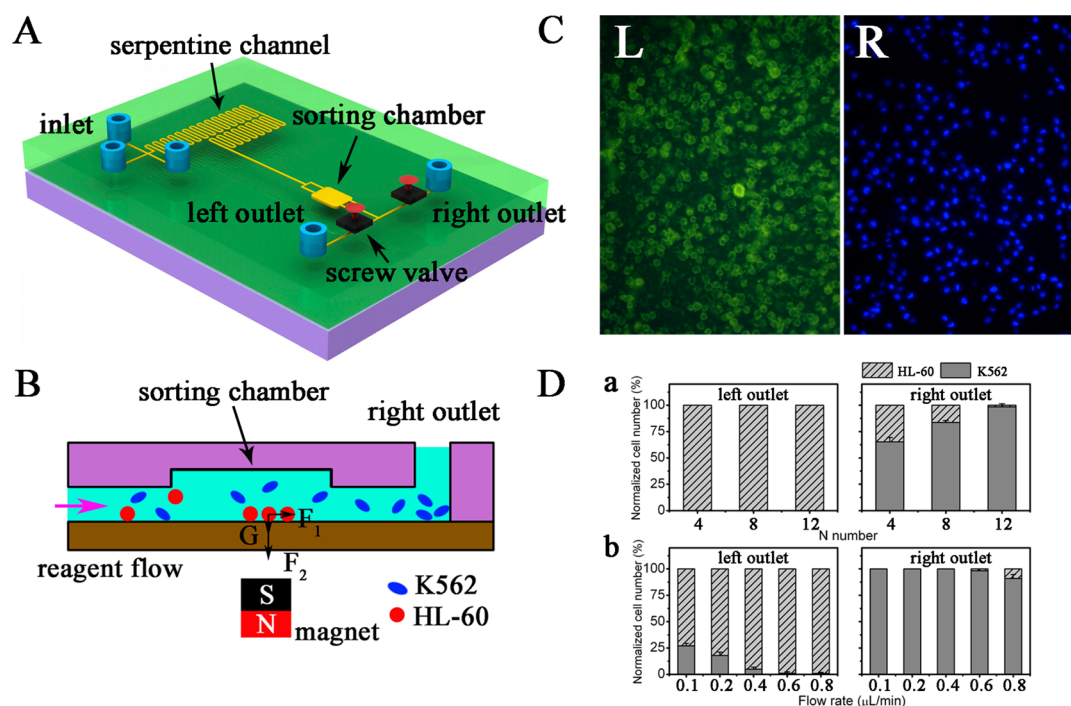
Figure 5. Sorting of tumor cells with PDMQDs-aptamer by a microfluidic chip. (A) Schematic diagram of the cell sorting chip. (B) Sorting mechanism in the sorting chamber. PDMQDs-aptamer, HL-60, and K562 cells were simultaneously loaded into the three inlets. Cells and nanoprobes were mixed and interacted in the serpentine channel. When the mixture passed through the sorting chamber, in the presence of an external permanent magnet, HL-60 cells were influenced by three kinds of forces, including fluid shear stress, gravity, and magnetic force, while K562 cells were only affected by fluid shear stress and gravity. (C) Fluorescence microscopy images of HL-60 and K562 cells with a complete separation in left (L) and right (R) outlets, respectively, under UV excitation. The yellow fluorescence of HL-60 was derived from PDMQDs nanoprobes, while the blue color of K562 was stained by Hoechst 33342 nucleic acid dye before isolation experiment. (D) Normalized cell numbers of HL-60 and K562 cells in the left outlet and right outlet after the on-chip cell sorting, respectively. Cell sorting parameters were optimized by adjusting (a) the number (N) of the repeated serpentine channel and (b) flow rate.

The fluorescent microscopic images in Figure 5C display that the PDMQDs nanoprobes can efficiently and specifically label the HL-60 cells in the microfluidic chip. In order to optimize the separation efficiency, incubation time and flow rate were taken into account. As shown in Figure 5D and Figure S9 of the Supporting Information, the increase in the repeated channel number (N) provides sufficient time for the combination of nanoprobes and HL-60 cells, leading to a more efficient separation. The decrease in flow rate could attain the same aim, but too slow flow rate generated small flow shear stress to carry K562 to the outlet. Thus, the N value of 12 and the flow rate of 0.6 μL min^{-1} were chosen as the optimized parameters, and 1.0×10^4 HL-60 cells were separated from a 2.0×10^4 cell mixture in 10 min with a separation efficiency of more than 98%. Furthermore, a conventional method based on a culture dish was also conducted to separate HL-60 cells from K562 cells under the magnet. As shown in Figure S10 of the Supporting Information, a prolonged incubation time (30 min) was needed in conventional method to achieve 90% separation efficiency, and more than 26% of HL-60 cells were lost during the repeated washing procedure to remove K562 cells. In comparison with the conventional method, microfluidic chip significantly shortened the experimental time, simplified the separating procedure and exhibited high separation efficiency.

CONCLUSIONS

A feasible method for the fabrication of specific tumor-targeting multi-functional nanoprobes was developed by employing $Fe_3O_4/SiO_2/CdSeTe@ZnS–SiO_2$ core/shell/shell nanostruc-

tures as magnetism and fluorescence carriers and using polydopamine shells as active media for conjugation with recognizing biomolecules. The fluorescence quenching effect was subtly circumvented by constructing the inner silica shell and outer polydopamine shell around the high-fluorescence QDs. Acting not only as a convenient bridge for linking the probe with biomolecules, the polydopamine coating layer also helped to lower the cytotoxicity. After the conjugation of the aptamer, the functionalized nanoprobes showed strong fluorescence and high selectivity and specificity in labeling the target epitopes expressed on the surfaces of HL-60 cells. Meanwhile, the nanoprobes were used to label and sort target cells from a homogeneous cell mixture on the basis of a microfluidic chip. Compared to a conventional magnetic separation method, the high separation efficiency could be achieved in a short separating time and by using a simple experimental procedure by microfluidic chip. As an integration of ultrastrong fluorescence emission and rapid magnetic response, the proposed nanoprobes are undoubtedly of significant value for optic monitoring of biological events and targeted separation of biomolecules and cells.

ASSOCIATED CONTENT

Supporting Information

XRD patterns of Fe_3O_4; quantum yields of QDs, MQDs, and PDMQDs; hydrodynamic diameters of $Fe_3O_4@SiO_2$, MQDs, DMQDs, PDMQDs-aptamer, and MQDs-dopamine; TEM image of DMQDs; long-term stability of DMQDs and PDMQDs; CLSM images of Hela incubated with DMQDs

7423

dx.doi.org/10.1021/am401740a | ACS Appl. Mater. Interfaces 2013, 5, 7417−7424

and PDMQDs; photostability of nanoprobes; CLSM images of cell sorting results; and conventional cell separation efficiency. This material is available free of charge via the Internet at http://pubs.acs.org.

■ AUTHOR INFORMATION

Corresponding Author
*Tel/Fax: +86 25 83597204. E-mail: jjzhu@nju.edu.cn.

Notes
The authors declare no competing financial interest.

■ REFERENCES

(1) Jemal, A.; Siegel, R.; Xu, J.; Ward, E. *CA-Cancer J. Clin.* **2010**, *60*, 277−300.
(2) Yang, P.; Xu, Q. Z.; Jin, S. Y.; Lu, Y.; Zhao, Y.; Yu, S. H. *Chem.—Eur. J.* **2012**, *18*, 9294−9299.
(3) Shimoni, O.; Postma, A.; Yan, Y.; Scott, A. M.; Heath, J. K.; Nice, E. C.; Zelikin, A. N.; Caruso, F. *ACS Nano* **2012**, *6*, 1463−1472.
(4) Ojea-Jiménez, I.; García-Fernández, L.; Lorenzo, J.; Puntes, V. F. *ACS Nano* **2012**, *6*, 7692−7702.
(5) Nycholat, C. M.; Rademacher, C.; Kawasaki, N.; Paulson, J. C. *J. Am. Chem. Soc.* **2012**, *134*, 15696−15699.
(6) Wang, J.; Karpus, J.; Zhao, B. S.; Luo, Z.; Chen, P. R.; He, C. *Angew. Chem., Int. Ed.* **2012**, *51*, 9652−9656.
(7) Yang, X.; Liu, X.; Liu, Z.; Pu, F.; Ren, J.; Qu, X. *Adv. Mater.* **2012**, *24*, 2890−2895.
(8) Cho, N. H.; Cheong, T. C.; Min, J. H.; Wu, J. H.; Lee, S. J.; Kim, D.; Yang, J. S.; Kim, S.; Kim, Y. K.; Seong, S. Y. *Nat. Nanotechnol.* **2011**, *6*, 675−682.
(9) Zhang, Q.; Liu, F.; Nguyen, K. T.; Ma, X.; Wang, X.; Xing, B.; Zhao, Y. *Adv. Funct. Mater.* **2012**, *22*, 5144−5156.
(10) Xie, H. Y.; Zuo, C.; Liu, Y.; Zhang, Z. L.; Pang, D. W.; Li, X. L.; Gong, J. P.; Dickinson, C.; Zhou, W. Z. *Small* **2005**, *1*, 506−509.
(11) Wang, D. S.; He, J. B.; Rosenzweig, N.; Rosenzweig, Z. *Nano Lett.* **2004**, *4*, 409−413.
(12) Cheng, L.; Yang, K.; Li, Y. G.; Zeng, X.; Shao, M. W.; Lee, S. T.; Liu, Z. *Biomaterials* **2012**, *33*, 2215−2222.
(13) Wu, W. Y.; Sun, Z. H.; Zhang, Y.; Xu, J.; Yu, H. S.; Liu, X.; Wang, Q.; Liu, W. S.; Tang, Y. *Chem. Commun.* **2012**, *48*, 11017−11019.
(14) Zhang, L. Y.; Wang, T. T.; Li, L.; Wang, C. G.; Su, Z. M.; Li, J. *Chem. Commun.* **2012**, *48*, 8706−8708.
(15) Selvan, S. T. *Biointerphases* **2010**, *5*, FA110−FA115.
(16) Hu, J.; Xie, M.; Wen, C. Y.; Zhang, Z. L.; Xie, H. Y.; Liu, A. A.; Chen, Y. Y.; Zhou, S. M.; Pang, D. W. *Biomaterials* **2011**, *32*, 1177−1184.
(17) Salgueiriño-Maceira, V.; Correa-Duarte, M. A.; Spasova, M.; Liz-Marzán, L. M.; Farle, M. *Adv. Funct. Mater.* **2006**, *16*, 509−514.
(18) Zhang, F.; Braun, G. B.; Pallaoro, A.; Zhang, Y.; Shi, Y.; Cui, D.; Moskovits, M.; Zhao, D.; Stucky, G. D. *Nano Lett.* **2011**, *12*, 61−67.
(19) Song, E. Q.; Hu, J.; Wen, C. Y.; Tian, Z. Q.; Yu, X.; Zhang, Z. L.; Shi, Y. B.; Pang, D. W. *ACS Nano* **2011**, *5*, 761−770.
(20) Di Corato, R.; Bigall, N. C.; Ragusa, A.; Dorfs, D.; Genovese, A.; Marotta, R.; Manna, L.; Pellegrino, T. *ACS Nano* **2011**, *5*, 1109−1121.
(21) Resch-Genger, U.; Grabolle, M.; Cavaliere-Jaricot, S.; Nitschke, R.; Nann, T. *Nat. Methods* **2008**, *5*, 763−775.
(22) Xie, M.; Hu, J.; Long, Y. M.; Zhang, Z. L.; Xie, H. Y.; Pang, D. W. *Biosens. Bioelectron.* **2009**, *24*, 1311−1317.
(23) Lee, H.; Rho, J.; Messersmith, P. B. *Adv. Mater.* **2009**, *21*, 431−434.

(24) Lee, H.; Dellatore, S. M.; Miller, W. M.; Messersmith, P. B. *Science* **2007**, *318*, 426−430.
(25) Ye, Q.; Zhou, F.; Liu, W. *Chem. Soc. Rev.* **2011**, *40*, 4244−4258.
(26) Xu, C. J.; Xu, K. M.; Gu, H. W.; Zheng, R. K.; Liu, H.; Zhang, X. X.; Guo, Z. H.; Xu, B. *J. Am. Chem. Soc.* **2004**, *126*, 9938−9939.
(27) Yan, J.; Yang, L. P.; Lin, M. F.; Ma, J.; Lu, X. H.; Lee, P. S. *Small* **2013**, *9*, 596−603.
(28) Park, J.; An, K.; Hwang, Y.; Park, J. G.; Noh, H. J.; Kim, J. Y.; Park, J. H.; Hwang, N. M.; Hyeon, T. *Nat. Mater.* **2004**, *3*, 891−895.
(29) Lin, Y. S.; Wu, S. H.; Hung, Y.; Chou, Y. H.; Chang, C.; Lin, M. L.; Tsai, C. P.; Mou, C. Y. *Chem. Mater.* **2006**, *18*, 5170−5172.
(30) Shen, Y. Y.; Li, L. L.; Lu, Q.; Ji, J.; Fei, R.; Zhang, J. R.; Abdel-Halim, E. S.; Zhu, J. J. *Chem. Commun.* **2012**, *48*, 2222−2224.
(31) Cao, J. T.; Chen, Z. X.; Hao, X. Y.; Zhang, P. H.; Zhu, J. J. *Anal. Chem.* **2012**, *84*, 10097−10104.
(32) Whitesides, G. M.; Hulme, S. E.; Shevkoplyas, S. S. *Lab Chip* **2009**, *9*, 79−86.
(33) Sathe, T. R.; Agrawal, A.; Nie, S. *Anal. Chem.* **2006**, *78*, 5627−5632.
(34) Lin, Y. S.; Haynes, C. L. *Chem. Mater.* **2009**, *21*, 3979−3986.
(35) Yi, D. K.; Lee, S. S.; Papaefthymiou, G. C.; Ying, J. Y. *Chem. Mater.* **2006**, *18*, 614−619.
(36) Sun, P.; Zhang, H.; Liu, C.; Fang, J.; Wang, M.; Chen, J.; Zhang, J.; Mao, C.; Xu, S. *Langmuir* **2010**, *26*, 1278−1284.
(37) Hong, S.; Na, Y. S.; Choi, S.; Song, I. T.; Kim, W. Y.; Lee, H. *Adv. Funct. Mater.* **2012**, *22*, 4711−4717.
(38) Malisova, B.; Tosatti, S.; Textor, M.; Gademann, K.; Zurcher, S. *Langmuir* **2010**, *26*, 4018−4026.
(39) Li, S. C.; Wang, J. G.; Jacobson, P.; Gong, X. Q.; Selloni, A.; Diebold, U. *J. Am. Chem. Soc.* **2009**, *131*, 980−984.
(40) Ham, H. O.; Liu, Z.; Lau, K. H. A.; Lee, H.; Messersmith, P. B. *Angew. Chem., Int. Ed.* **2011**, *50*, 732−736.
(41) Luo, Y.; Wang, C. M.; Hossain, M.; Qiao, Y.; Ma, L. Y.; An, J. C.; Su, M. *Anal. Chem.* **2012**, *84*, 6731−6738.
(42) Reichert, J. M.; Valge-Archer, V. E. *Nat. Rev. Drug Discovery* **2007**, *6*, 349−356.
(43) Sefah, K.; Tang, Z. W.; Shangguan, D. H.; Chen, H.; Lopez-Colon, D.; Li, Y.; Parekh, P.; Martin, J.; Meng, L.; Phillips, J. A.; Kim, Y. M.; Tan, W. H. *Leukemia* **2009**, *23*, 235−244.
(44) Thiel, A.; Scheffold, A.; Radbruch, A. *Immunotechnology* **1998**, *4*, 89−96.
(45) McCloskey, K. E.; Chalmers, J. J.; Zborowski, M. *Anal. Chem.* **2003**, *75*, 6868−6874.
(46) Tong, X.; Xiong, Y.; Zborowski, M.; Farag, S. S.; Chalmers, J. J. *Exp. Hematol.* **2007**, *35*, 1613−1622.
(47) Gijs, M. A. M.; Lacharme, F.; Lehmann, U. *Chem. Rev.* **2010**, *110*, 1518−1563.
(48) Browne, A. W.; Ramasamy, L.; Cripe, T. P.; Ahn, C. H. *Lab Chip* **2011**, *11*, 2440−2446.
(49) Pamme, N.; Wilhelm, C. *Lab Chip* **2006**, *6*, 974−980.
(50) Shafiee, H.; Sano, M. B.; Henslee, E. A.; Caldwell, J. L.; Davalos, R. V. *Lab Chip* **2010**, *10*, 438−445.
(51) Lien, K. Y.; Chuang, Y. H.; Hung, L. Y.; Hsu, K. F.; Lai, W. W.; Ho, C. L.; Chou, C. Y.; Lee, G. B. *Lab Chip* **2010**, *10*, 2875−2886.
(52) Fan, Z. H.; Xu, Y.; Phillips, J. A.; Yan, J. L.; Li, Q. G.; Tan, W. H. *Anal. Chem.* **2009**, *81*, 7436−7442.
(53) Beech, J. P.; Holm, S. H.; Adolfsson, K.; Tegenfeldt, J. O. *Lab Chip* **2012**, *12*, 1048−1051.
(54) Liu, R. H.; Stremler, M. A.; Sharp, K. V.; Olsen, M. G.; Santiago, J. G.; Adrian, R. J.; Aref, H.; Beebe, D. J. *J. Microelectromech. Syst.* **2000**, *9*, 190−197.

7424

dx.doi.org/10.1021/am401740a | *ACS Appl. Mater. Interfaces* 2013, 5, 7417−7424